Structural Basis for the Subversion of MAP Kinase Signaling by an Intrinsically Disordered Parasite Secreted Agonist

Erika Pellegrini, Andres Palencia, Laurence Braun, Ulrike Kapp, Alexandre Bougdour, Hassan Belrhali, Matthew W. Bowler, Mohamed-Ali Hakimi

CellPress

Structure
Article

Structural Basis for the Subversion of MAP Kinase Signaling by an Intrinsically Disordered Parasite Secreted Agonist

Erika Pellegrini,[1,2] Andrés Palencia,[3] Laurence Braun,[3] Ulrike Kapp,[4] Alexandre Bougdour,[3] Hassan Belrhali,[1,2,*] Matthew W. Bowler,[1,2,*] and Mohamed-Ali Hakimi[3,5,*]

[1]European Molecular Biology Laboratory, Grenoble Outstation, 71 Avenue des Martyrs, CS 90181, 38042 Grenoble, France
[2]Unit for Virus Host Cell Interactions, Université Grenoble Alpes-EMBL-CNRS, 71 Avenue des Martyrs, CS 90181, 38042 Grenoble, France
[3]IAB, Team Host-Pathogen Interactions & Immunity to Infection, INSERM U1209, CNRS UMR5309, Université Grenoble Alpes, 38700 Grenoble, France
[4]Structural Biology Group, European Synchrotron Radiation Facility, 71 Avenue des Martyrs, CS 90181, 38042 Grenoble, France
[5]Lead Contact
*Correspondence: belrhali@embl.fr (H.B.), mbowler@embl.fr (M.W.B.), mohamed-ali.hakimi@univ-grenoble-alpes.fr (M.-A.H.)
http://dx.doi.org/10.1016/j.str.2016.10.011

SUMMARY

The causative agent of toxoplasmosis, the intracellular parasite *Toxoplasma gondii*, delivers a protein, GRA24, into the cells it infects that interacts with the mitogen-activated protein (MAP) kinase p38α (MAPK14), leading to activation and nuclear translocation of the host kinase and a subsequent inflammatory response that controls the progress of the parasite. The purification of a recombinant complex of GRA24 and human p38α has allowed the molecular basis of this activation to be determined. GRA24 is shown to be intrinsically disordered, binding two kinases that act independently, and is the only factor required to bypass the canonical mitogen-activated protein kinase activation pathway. An adapted kinase interaction motif (KIM) forms a highly stable complex that competes with cytoplasmic regulatory partners. In addition, the recombinant complex forms a powerful in vitro tool to evaluate the specificity and effectiveness of p38α inhibitors that have advanced to clinical trials, as it provides a hitherto unavailable stable and highly active form of p38α.

INTRODUCTION

A critical issue for the immune system in mammals is to achieve a balance between protection and immune pathology. Much research has focused on the regulatory mechanisms of this balance and their dysfunction in a number of disease settings. In the specific setting of host infection and intracellular pathogens, it has been found that a wide range of pathogens directly hijack the immunoregulatory network during the course of infection. In the case of the Apicomplexa protozoan *Toxoplasma gondii*, the parasite has evolved methods to trigger a transient innate proinflammatory response that guarantees both control of the parasite population and survival of the host, promoting the establishment of a persistent cryptic parasite population (i.e., parasite survival) (Hunter and Sibley, 2012). Like most pathogens, it has evolved numerous methods of hijacking cell-signaling pathways in order to survive in the host cell. As an obligate intracellular protozoan, it delivers effector proteins into its host cell (Hakimi and Bougdour, 2015; Melo et al., 2011) to control mitogen-activated protein kinase (MAPK) signaling in macrophages, which in turn dictate parasite burden and disease (Braun et al., 2013; Kim et al., 2005). MAPK signaling is characterized by a cascade of multiple kinases, through which the signal is transduced in the form of phosphorylation events from an upstream kinase to a downstream one (Chen et al., 2001; Johnson and Lapadat, 2002). The final phosphorylation event is a dual phosphorylation, which occurs on a conserved Thr-X-Tyr motif in the activation loop (AL) of the MAPK (Cobb and Goldsmith, 1995; Davis, 1995). The phospho-residues are then able to bind basic patches, changing the relative orientation from open in the inactive state to closed in the active state allowing nucleotide binding in the active site (Jura et al., 2011; Kornev and Taylor, 2010).

One of the effector proteins secreted by *T. gondii*, GRA24, has been shown to interact with the MAP kinase p38α, promoting its activation and nuclear translocation (Braun et al., 2013). GRA24 encodes a 542 amino acid protein with an internal putative bipartite nuclear localization signal, and two repeats, R1 and R2, at the C terminus (Figure 1A). The mechanism by which GRA24 activates p38α, either directly or by modulating the existing activation pathway, is unknown. Previous experiments that mapped the region of the interactions between the two proteins in infected cells show that only one of the repeats is essential for the activation of p38α. Through a docking model, it was proposed that binding of p38α by GRA24 is driven by the kinase interaction motif (KIM), embedded in each of the two repeat regions (Figure 1A). KIMs are linear motifs used by kinases, phosphatases, substrates, and scaffold proteins to bind MAPKs at the KIM or D-motif binding site and regulate their activity (Enslen et al., 2000; Kallunki et al., 1996; Zuniga et al., 1999). KIMs ensure specificity between partners but also have allosteric effects on the proteins (De Nicola et al., 2013; Tokunaga et al., 2014; Zhou et al., 2006).

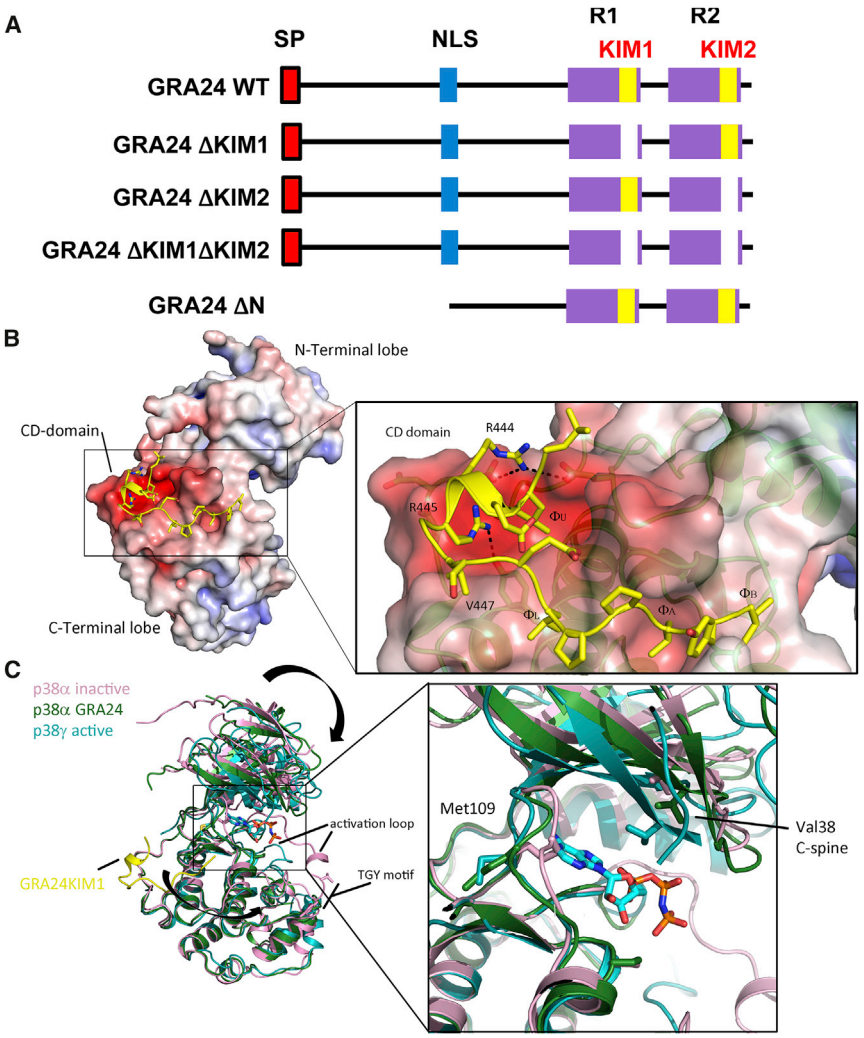

Figure 1. Structure of the GRA24KIM1-p38α Complex

(A) Diagram of GRA24, KIM deletion mutants, and N-terminally truncated constructs used in this study. Signal peptide (red), nuclear localization signal (blue), internal repeats (purple), and KIM (yellow) sequences are shown.

(B) The structure of p38α is shown as a solvent accessible surface colored by electrostatic potential (−10 to 10 kTe^{-1}, red to blue) and the GRA24KIM1 peptide is shown in cartoon representation with side chains as sticks (yellow). Details of the interactions between p38α and GRA24KIM1 are inset. GRA24 uses all the classical interactions (ϕ_A, ϕ_B, ϕ_L, ϕ_U, and RR) as well as an additional hydrophobic interaction with V447.

(C) Conformational changes induced by GRA24-KIM1 binding allow nucleotide entry to the active site (inactive conformation PDB: 5ETC, active conformation PDB: 1CM8). The rearrangement of the C-spine (Val38, Ala51, Ala157, Leu156, Val158, Leu113, Ile212, and Leu216) from the inactive to active state is highlighted by the movement of Val38.

Here, we have produced a recombinant complex of an N-terminal truncation of GRA24 (GRA24ΔN, Figure 1A) and p38α. Using a combinatorial approach of various structural techniques, the macrostructure of the recombinant complex between GRA24 and p38α and the crystal structure of the core interaction between the proteins is described. The results provide a molecular view of activation and define GRA24 as the only component required to activate p38α. The recombinant complex of GRA24 and p38α also provides a highly specific tool to determine the activity of p38α inhibitors that have advanced to clinical trials.

RESULTS

Structure of the GRA24KIM1-p38α Complex

To define the molecular basis of the interaction between p38α and GRA24, we determined the crystal structure of p38α bound to the GRA24 KIM1 peptide (residues 440–455) at 2.8 Å (Table 1). The complex crystallized in the triclinic space group *P*1 with two molecules in the asymmetric unit. The electron density for the GRA24KIM1-p38α complex was excellent and the entire peptide sequence could be traced (Figure S1A). As the density is slightly better in the second molecule (chain B), only this chain is used in subsequent descriptions. KIMs have a general consensus sequence of X-ϕ_U-X_2-(θ(Arg/Lys))$_{1-2}$-$(X)_{2-6}$-ϕ_L-$(X)_{1-2}$-ϕ_A-X-ϕ_B (where ϕ_A, ϕ_B, ϕ_L, and ϕ_U are hydrophobic residues [usually Leu, Ile, or Val] and θ is a basic residue [Arg or Lys]) (Gavin and Nebreda, 1999; Smith et al., 1999), shorter motifs can lack the first four residues (Sharrocks et al., 2000; Zeke et al., 2015). The KIM or D-motif binding site is formed by an acidic patch known as the common docking (CD) domain (Tanoue et al., 2001) and a hydrophobic docking groove (Chang et al., 2002; Gum and Young, 1999) (Figure 1B). The CD domain accommodates the ϕ_U and basic residues, while the hydrophobic docking groove binds ϕ_A, ϕ_B, and ϕ_L (Akella et al., 2010; Heo et al., 2004; Lee et al., 2006). The GRA24 peptide binds with the hydrophobic residues (Φ_A-Φ_B) in the docking groove formed by α_d and α_e and the reverse turn between β_7 and β_8 in the C-terminal lobe of p38α (Figure 1B). Moreover, GRA24 utilizes all interacting motifs identified so far (Peti and Page, 2013; Zeke et al., 2015), including the additional hydrophobic residues, Φ_L and Φ_U, and the ionic contacts with the p38α CD domain, where the KIM1 peptide forms a short α helix involving residues RRELLG (Figure 1B). An additional hydrophobic interaction, not observed in other KIMs, is made with V447. Binding of GRA24KIM1 causes significant conformational change and disorder in the AL with a rotation of the N-terminal domain of 10° toward the C-terminal domain caused by tightening between the areas linked by the peptide (Figure 1C). This movement results in the alignment of the catalytic spine (C-spine) toward the active state, one of the essential events in kinase activation (McClendon et al., 2014), the residues belonging to the C-spine and the hinge region are in a similar position to the fully activated ATP bound p38γ (Bellon et al., 1999) (Figure 1C). The

Table 1. Data Processing and Refinement Statistics for the GRA24KIM1-p38α and MKK6KIM-p38αK53R Structures

Structure	GRA24KIM-p38α (5ETA)	MKK6KIM-p38αK53R (5ETF)
Data Collection		
Space group	*P*1	$P3_121$
Unit cell dimensions		
a, b, c (Å)	52.0, 61.9, 75.7	82.4, 82.4, 123.3
α, β, γ (°)	105.6, 96.3, 114.7	90.0, 90.0, 120.0
Resolution range (Å)	45.79 (2.95–2.8)	46.65 (2.49–2.4)
R_{meas}	0.09 (0.27)	0.108 (0.690)
$\langle I/\sigma(I)\rangle$	9.9 (3.0)	13.3 (2.1)
Redundancy	1.9 (1.9)	3.9 (3.9)
Completeness (%)	96.5 (97.2)	90.3 (59.0)
Refinement		
Resolution range (Å)	20.0 (2.95–2.8)	20.0 (2.49–2.4)
No. of reflections	36,372	32,069
R_{work}/R_{free}	22.3/28.3	16.29/23.1
No. of atoms		
Protein	2,715 (A), 2,705 (B)	2,725
	127 (C), 127 (D) GRA24KIM1	92 (MKK6KIM)
Water	29	223
B factors (Å^2)		
Protein	63.69 (A), 59.98 (B)	32.25
Ligand	73.97 (C), 83.91 (D)	42.33
Water	46.87	33.48
RMSD		
Bond lengths (Å)	0.006	0.0078
Bond angles (°)	1.113	0.931
Ramachandran favored (%)	95.8	97.7
Ramachandran outliers (%)	0.4	0
Rotamer outliers (%)	2.2	1.3
Clash score	9.68	4.82
Overall score	2.07	1.41

Values in parentheses are for the outer resolution shell.
RMSD, root-mean-square deviation.

rearrangement also leads to a rotation of methionine 109 in the hinge region that prevents nucleotide binding in the active site of the inactive protein (Figure 1C). These conformational changes would allow the entry of ATP into the active site and make the AL accessible for phosphorylation between activated p38α molecules.

GRA24 Has High Affinity for p38α by Combining the Attributes of Different KIM Domains

To further characterize the interaction between GRA24 and p38α we compared the binding of GRA24 KIM1 with other KIM peptides described in the literature (Table S1) using isothermal calorimetry (ITC). The GRA24 KIM1 peptide was found to bind p38α with an equilibrium dissociation constant (K_D) of 1.6 μM (Table S1 and Figure S2), ~2-fold tighter than KIMs found in phosphatases, which have the highest measured affinity of cytosolic regulatory partners involved in classical MAPK regulation (Francis et al., 2011). While the full-length proteins may show different affinities and binding modes, these results show that the GRA24 KIM has a higher affinity than either upstream kinases or downstream phosphatase KIMs.

The GRA24KIM1-p38α structure shows that high-affinity and allosteric effects (disorder of the AL) is achieved by combining the sequences of both the upstream MKK KIMs and those of the downstream phosphatases (Figures 2B, 2C, and S3). To compare binding by an upstream kinase we determined a complex of a kinase dead mutant and the KIM domain from MKK6 (residues 4–18) at 2.4 Å (MKK6KIM-p38αK53R, Table 1) with no mutation in the KIM binding area, as there is in a published structure (C162S) (Garai et al., 2012). The complex crystallized in the trigonal $P3_121$ space group with one molecule in the asymmetric unit. Comparison of the structures shows GRA24 binding in a similar manner to the hydrophobic groove, using the same L and I residues for Φ_A-Φ_B but, unusually, uses the hydrophobic base of arginine in the Φ_L pocket (Figure 2C). This is a longer linker between Φ_L and Φ_B pockets than predicted and is more similar to the GRA24 KIM that has a double proline spacer. There is no interaction with the CD domain or the associated secondary structural rearrangement (Figure S1B). None of the MAPKK-p38α structures available show binding to the CD domain. However, GRA24KIM1 binding to the p38α CD domain is similar to that described for tyrosine phosphatases (Figure 2B), the KIMs of which comprise an RR motif usually structured in a short α helix (Zhou et al., 2006).

The only KIM with a higher affinity for p38α is from the MAPK substrate MAPKAP kinase 2 (K_D of 50 nM; Garai et al., 2012). As MAPKAPK2 is only present in the nucleus (Zakowski et al., 2004) it will not compete with recruitment of p38α by GRA24 in the cytoplasm. Nevertheless, it is interesting to note that the GRA24 KIM1 has a very similar mode of binding to the MAPKAP2 KIM, both in the hydrophobic groove and to the CD domain, leading to very tight binding (Figure 2E). The major difference between the two KIMs is the reverse direction of the MAPKAP2 sequence (Figure S3, C- to N-terminal) and increased secondary structure elements (Figure 2E).

The Structure of the GRA24ΔN-p38α Complex Shows Two Independent Kinases Bound to an Intrinsically Disordered Protein

To define the mechanism of activation of p38α by GRA24 the complex between the proteins must be studied; we therefore attempted to produce the protein in *Escherichia coli*. Expression of either the wild-type (WT) or a truncation removing the N terminus to the nuclear localization sequence (GRA24ΔN, residues 337–542, Figure 1A) failed to produce detectable expression. However, when co-expressed with p38α, a stable complex between p38α and GRA24ΔN was produced (Figure S4) as the association with the kinase presumably prevents proteolysis. The complex was purified to homogeneity and analysis of staining intensity indicated a ratio of 1:2 for GRA24ΔN to p38α. We then investigated the structure of the complex using small-angle X-ray scattering (SAXS). SAXS was used to determine the average structure of the GRA24ΔN-p38α complex in solution (Table S2). The radius of gyration was determined to be 4.85 nm

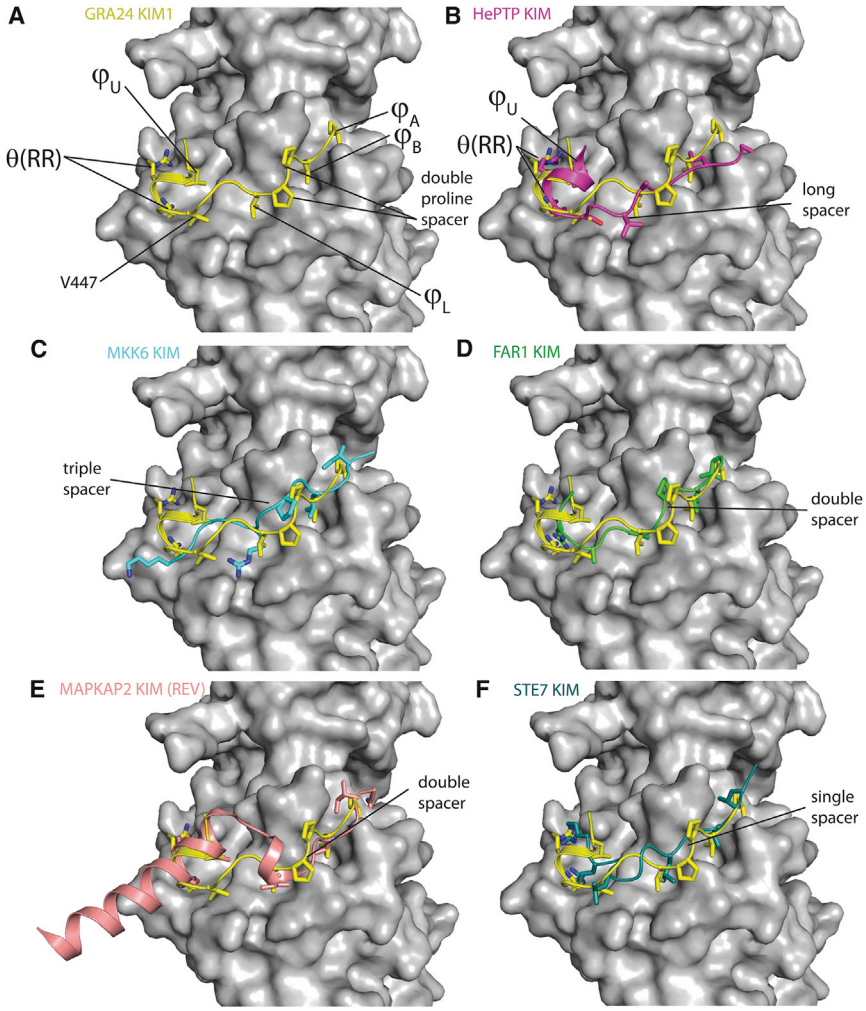

Figure 2. Comparison of the Binding Modes of KIMs

(A) The GRA24 KIM. Residues that interact directly are shown as sticks.

(B) Comparison with the phosphatase PTP KIM, GRA24, and the PTP KIM have a very similar binding to the CD domain with the ϕ_U and RR residues but diverge as the hydrophobic groove is approached.

(C) Comparison with the p38-activating kinase MKK6 KIM: similar binding is observed in the hydrophobic groove with a larger space between the ϕ_B and ϕ_L pockets.

(D) Comparison with the yeast MAPK substrate Far1 KIM, a very similar mode of binding is observed that only diverges at the CD domain.

(E) Comparison with the p38 substrate MAPKAP2 KIM that has the highest affinity and runs C- to N-terminal left to right. The interactions are very similar despite the additional secondary structure and reverse binding.

(F) Comparison with the yeast Ste7 KIM. The two KIMs are very similar in sequence but binding diverges slightly at the CD domain. See also Figures S3 and S5.

with a D_{max} of 16.96 nm and ab initio modeling showing an elongated molecule (Figures 3A and 3B) best described by a disordered protein binding two globular domains. The pair distribution function (Figure 3A, inset) also suggests flexibility between the kinases (full width at half maximum of 3.8–6.2 nm about the mode of 4.85 nm) implying disorder in GRA24. The possibility that the dimer observed in the crystal structure could also be present in solution was tested by SAXS (Table S2) and found to be a crystallization artifact.

Using the crystal structure of the GRA24KIM1-p38α complex and modeling GRA24 as an intrinsically disordered protein, a structure of the complex can be proposed (Figures 3B and 3C). The refined model is an excellent fit to the experimental curve ($\chi^2 = 1.08$) and provides insight into its mode of action (Figures 3A–3C). The two kinases are bound at the C terminus of GRA24, linked by ~65 residues.

Dimerization has been demonstrated to be part of an activating mechanism for p38α and its close homolog ERK2 (Diskin et al., 2007; Khokhlatchev et al., 1998). The presence of two KIMs in GRA24 opens the possibility that dimerization between the bound kinases could play a role in activation. The SAXS data imply movement between the kinases; however, as it only provides an average envelope of the structure the relationship between the kinases cannot be fully defined. We therefore used single-molecule approaches, negative-stain electron microscopy (EM), and atomic force microscopy (AFM), to investigate the dynamics of the complex. EM confirmed the flexibility, with class averages showing the two kinases in close proximity, but with a considerable variety of positions (Figure 3D). AFM also shows the dynamic nature of the complex at the single-molecule level (Figure 3E). In both AFM and EM data no secondary structure can be observed in GRA24 confirming its disordered nature. These data demonstrate flexibility between the kinases, eliminating the possibility of a dimer, which implies that the kinases can act independently.

We therefore tested the requirement in vivo of each of the KIMs specifically, by developing 293 derived inducible stable cell lines expressing hemagglutinin (HA) Flag-tagged GRA24 where either KIM1, KIM2, or both KIMs were mutated to alanine (Figure 1A). Immunoblotting for phosphorylated p38α demonstrates that GRA24 induces phosphorylation with only one KIM, but at least one is required for activity as the double mutant leads to an absence of activated p38α (Figure 4A). This is in agreement with previous results demonstrating that a single internal repeat domain was required for activation (Braun et al., 2013). This result defines the GRA24-KIM as the essential factor in the recruitment and activation of p38α in vivo and that dimerization of the kinases is not required for activation.

The Recombinant Complex Is Active and Provides a Tool to Assess p38α Inhibitors

The activity of the complex was assessed by assaying its ability to phosphorylate itself (Figure 4B) and also a typical transcription

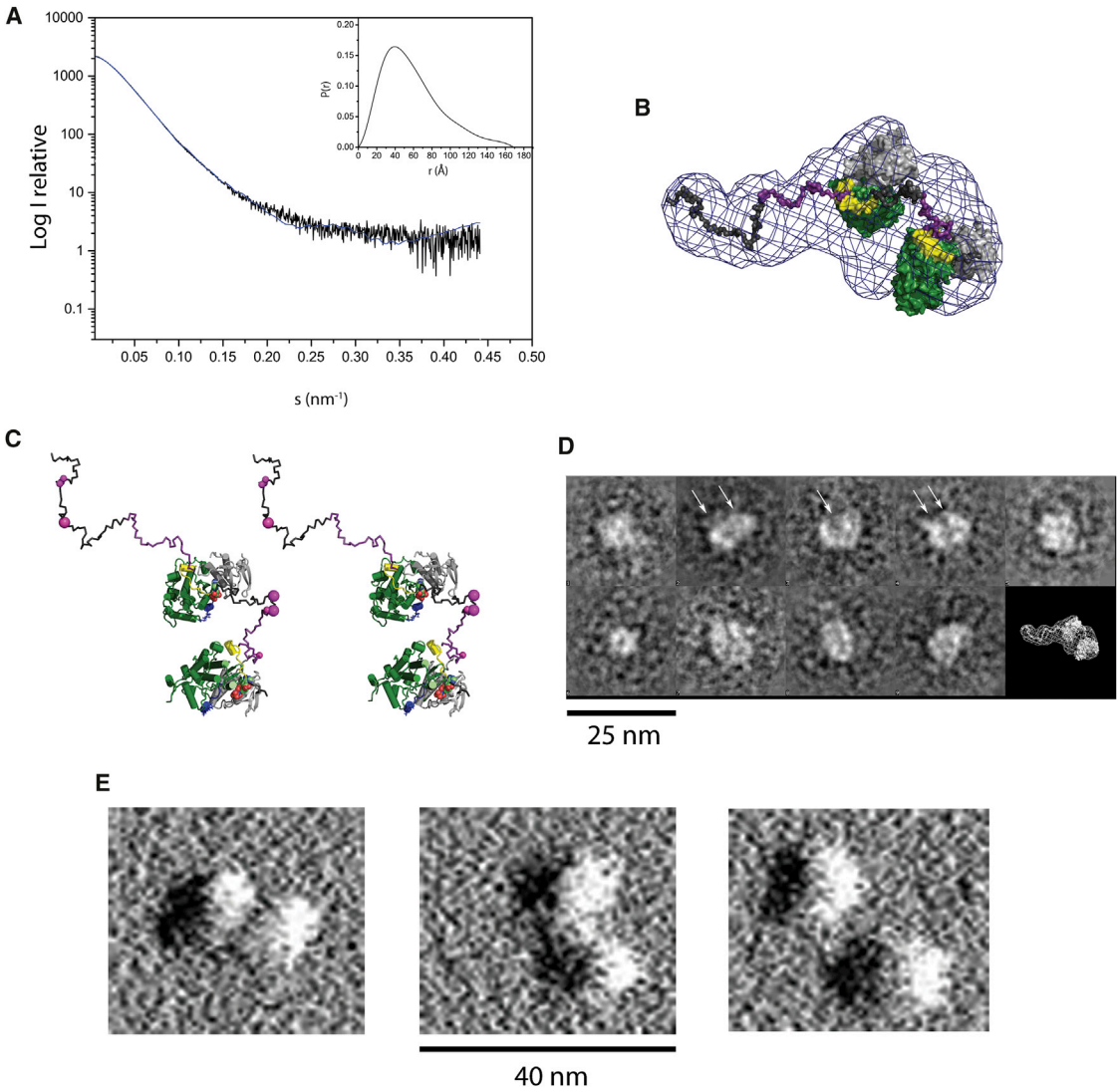

Figure 3. Structure of the GRA24ΔN-p38α Complex

(A) Scattering curve of the GRA24ΔN-p38α complex: the fit of models (B) and (C) is shown in blue and the pair distribution function is shown in the inset.

(B) Ab initio model of the GRA24ΔN-p38α complex (blue mesh) with the final model (internal repeats, purple; KIM, yellow; p38α is shown with N-terminal lobes in gray, C-terminal in green, and AL in blue).

(C) Model of the GRA24ΔN-p38α complex, colored as in (B), in stereo showing phosphorylation sites (magenta) identified by mass spectrometry (Table S3) scaled according to the number of times found.

(D) Class averages from negative-stain EM of the GRA24ΔN-p38α complex. Arrows indicate class averages where the two p38α molecules are separated; considerable variety in the orientation of the two kinases is observed. The SAXS model is shown to scale for reference.

(E) The GRA24ΔN-p38α complex visualized by AFM, kinase pairs are observed in multiple conformations.

factor target of p38α, activating transcription factor 2 (ATF2) (Figure 4C). Incubation of the complex with radiolabeled ATP demonstrates the complex is active (Figure 4B) and mass spectrometry shows that phosphorylation occurs on multiple serine and threonine residues within GRA24 (Table S3, Figure 3C), including a previously identified kinase motif (Braun et al., 2013). Assaying the complex's activity against a natural target, ATF2, shows that p38α in complex with GRA24ΔN is significantly more active against ATF2 than p38α alone (Figure 4C). As both proteins were expressed in *E. coli*, devoid of endogenous protein kinases, this defines GRA24ΔN as the only factor required to activate p38α and demonstrates that the complex is a powerful tool to unambiguously evaluate the pharmacological inhibition of p38α in vitro. A highly active and stable recombinant form of p38α is not currently available, hampering efforts to assay the specific effects of molecules on p38α. Using the GRA24ΔN-p38α complex, we have shown that many of the inhibitors developed against p38α, some of which are currently in phase II clinical trials, prevent ATF2 phosphorylation by the complex in vitro (Figure 4C). The ability of the compounds to impair p38α phosphorylation, in a GRA24-dependent manner, and concomitant epidermal growth factor 1 (EGR1) activation was

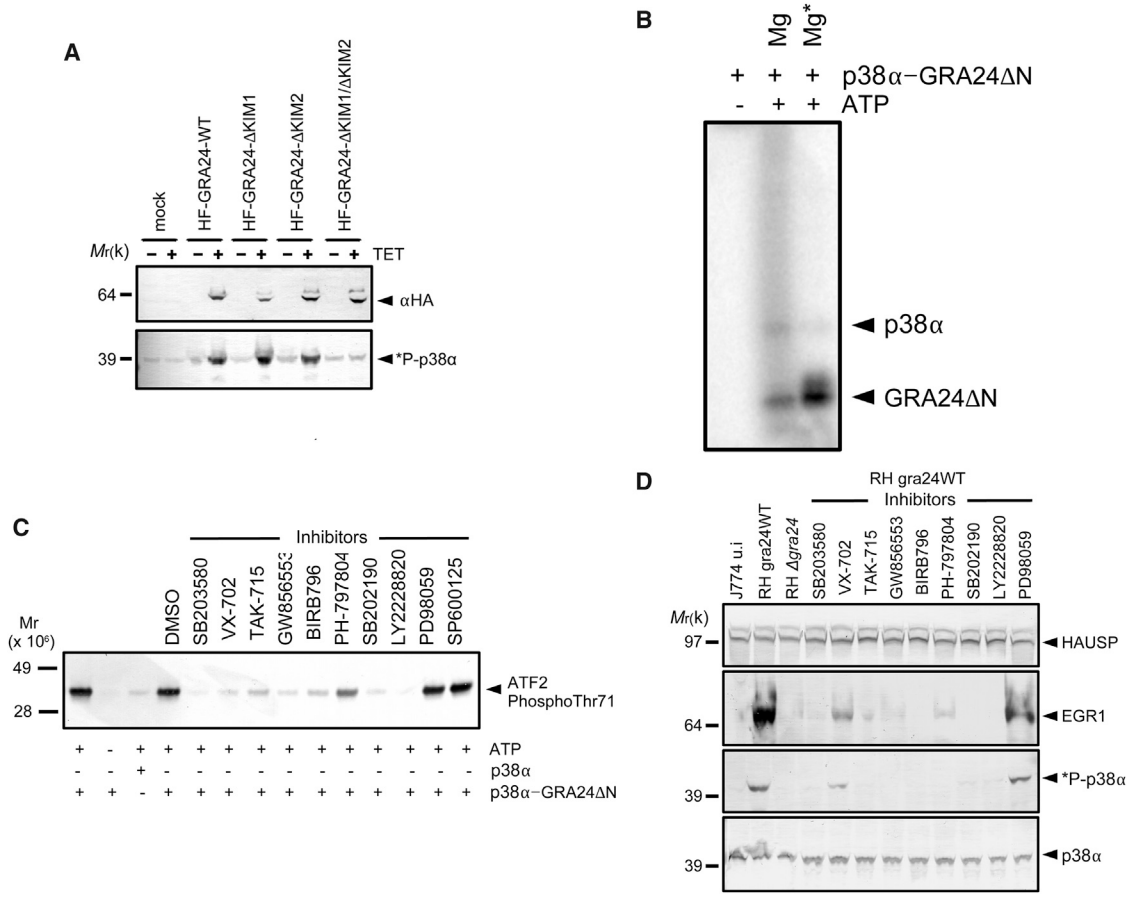

Figure 4. Activity of the GRA24ΔN-p38α Complex

(A) p38α phosphorylation in 293-TRex cells stably expressing GRA24 WT or KIM mutants. Nuclear fractions were immunoblotted with the indicated antibodies. Data are representative of three experiments.

(B) Auto-phosporylation of the GRA24ΔN-p38α complex was analyzed using a radioactivity-based assay, the third lane (Mg*) was treated with λ-phosphatase before the assay.

(C) Analysis of p38α MAP kinase activity by western blot using Phospho-ATF-2 (Thr71) Antibody and its inhibition by known kinase inhibitors. A selection of p38α inhibitors is shown to have a variety of effects on the inhibition of target phosphorylation. Inhibitors of upstream MKKs and JNK (PD98059 and SP600125) are shown as controls.

(D) Specific pharmacological inhibition of GRA24-dependent p38α phosphorylation in J774 MØ. Cells infected with WT or *Δgra24* KO parasites were incubated for 18 hr with p38 inhibitors (15 μM), control SAPK/JNK (SP600125, 25 μM), and MKK (PD98059, 15 μM) inhibitors as well as DMSO vehicle. Nuclear fractions were immunoblotted with the indicated antibodies.

validated in infected macrophages (Figure 4D). Differences in the observed inhibition between in vivo and in vitro assays, as well as between different inhibitors (Figures 4C and 4D), demonstrate the importance of having a permanently active form of p38α.

DISCUSSION

Pathogens often evolve methods of modulating host cell-signaling pathways in order to promote their growth and persistence in the infected cell. One of the most efficient methods to interact with host signaling proteins is the use of intrinsically disordered proteins combined with short linear motifs, as the evolutionary timescales involved are shorter than those required for globular domains (Davey et al., 2012; Fuxreiter et al., 2007; Hagai et al., 2014). Short linear motifs in particular can be used to allow interactions between a pathogenic protein and that of a host in a simple manner (Elde and Malik, 2009). This study demonstrates the molecular basis by which the parasite-derived agonist GRA24 bypasses the classical MAPK phosphorylation cascade and induces p38α auto-phosphorylation, forming an active complex able to activate transcription factors, such as ATF2.

The parasite protein operates through two atypical KIMs, embedded in an intrinsically disordered protein, which combine attributes of docking domains from multiple MAPK partners to maximize binding. A recent study has analyzed all known KIMs, identified many novel sequences, and classified them by their binding modes (Zeke et al., 2015). Differences are defined in the spacing between hydrophobic residues and the linker between the CD binding region and the docking groove region. Intriguingly, the GRA24 KIM borrows attributes from all the defined classes but does not fit in a single class (Figures 2, S3,

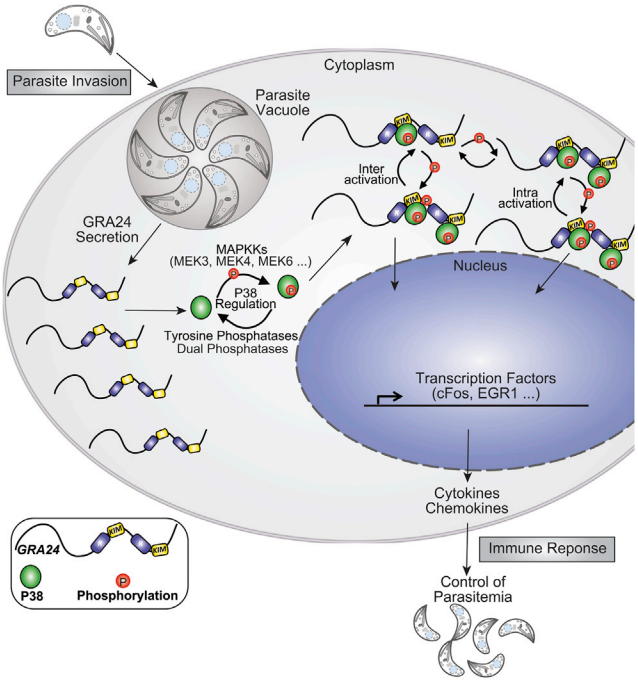

Figure 5. Model of How GRA24 Subverts MAP Kinase Signaling

GRA24 is secreted from the parasitophorous vacuole into the host cell cytoplasm where its high-affinity KIM sequence will recruit p38α. On binding GRA24, p38α is sequestered from regulatory kinases and phosphatases and can bind ATP allowing phosphorylation of the activation loop between and within complexes. The p38α-GRA24 complex is now a highly efficient active complex that can be translocated to the nucleus allowing a sustained and regular inflammatory response.

and S5). Overall, it is closest to the HePTP class incorporating all hydrophobic residues as well as the short helix bound to the CD domain. Interestingly, its linker is the same length as the KIM from Ste7 (Figure 2F), and its binding mode for the hydrophobic groove exactly the same as that for Far1 (Figure 2D) with a larger spacer between the Φ_L and Φ_B pockets (double proline) (Figures 1, 2, S3, and S5). Ste7 and Far1 are an activator and substrate, respectively, of yeast mating decision MAPKs, and the KIMs have no known higher eukaryotic equivalent. It is interesting to note that the binding mode of the GRA24 KIM is most similar to a unicellular eukaryote interaction pathway. KIMs perform many roles in the MAP kinase cascade, being present in upstream activating kinases, scaffold proteins, and deactivating phosphatases. Each partner uses the KIM to ensure specificity and control the protein allosterically. For example, the KIM from MKK6 loosely associates the two kinases and induces disorder in the AL making it available for phosphorylation. In contrast, phosphatase KIMs bind tightly and change the conformation of the AL to present the phospho-residues for dephosphorylation (Zhou et al., 2006). The first interaction must be transient to allow activated p38α to enter the nucleus and act on substrates, while the second must be long lived in order to tightly control the signal. On transport of the protein into the host cytoplasm the GRA24 KIMs will compete with the KIMs from regulatory pathways and induce conformational changes that allow ATP binding and the availability of the AL for *trans*-phosphorylation (Figure 5). The GRA24KIM-p38α structure shows that, in contrast to the so called third conformation of p38α (Akella et al., 2010) or the conformation induced by TAB1 for *cis*-phosphorylation (De Nicola et al., 2013), the kinase structure is very close to the active p38α and distinct from the inactive state. *trans*-Phosphorylation could occur both between the two kinase molecules bound to GRA24 and among kinases bound by different GRA24 molecules as in vivo data show that one R repeat is enough to promote p38α auto-phosphorylation (Figure 4). While two copies of the kinase are not necessary for activation, the possibility of phosphorylation between GRA24 kinase twins could enhance activity in a similar manner to scaffolding proteins (Brown and Sacks, 2009). GRA24 is itself then phosphorylated at multiple sites. Whether this has functional relevance or is just the result of an active kinase is not known, but a kinase recognition motif located between the bound kinases is highly phosphorylated, as are multiple serine and threonine residues throughout the protein (Figure 3C). Phosphorylation has been shown to play a role in protection of proteins from cellular proteases (Desagher et al., 2001; Døskeland et al., 1996) and also in nuclear translocation (Nardozzi et al., 2010), which could assist GRA24 in its role. At the N terminus, the rest of the protein is free, exposing the signal sequence to the nuclear transport machinery and allow the complex to be imported to the nucleus where it can act on specific transcription factors (Figure 5) (Braun et al., 2013). The structural features described here show how high-affinity binding to p38α by GRA24 prevents deactivation by phosphatases and promotes a sustained host kinase activation during *Toxoplasma* infection. The tight control of the inflammatory signaling prevents either too weak a response leading to host death or too strong a response preventing invasion.

Following pathogen infection or tissue damage, p38α induces the expression of multiple genes that together regulate the inflammatory response. Therefore, interference in p38α kinase activity could aid in therapy for inflammatory disorders ranging from rheumatoid arthritis to chronic obstructive pulmonary disease. Compounds targeting p38α must be highly selective in order to avoid adverse side effects triggered by off-target kinase inhibition. Although in vitro p38 inhibition assays exist, they are hampered by the need to activate the MAPK either in vivo, e.g., following lipopolysaccharide treatment, or through in vitro MKK6 *trans*-phosphorylation (Szafranska et al., 2005) and the short lived nature of the activated enzyme. By promoting a long-lasting activation of p38α, GRA24 challenges the natural-negative-feedback mechanisms that prevent the MAPK activation ad infinitum and offers a powerful in vitro tool to screen for small-molecule p38α inhibitors.

EXPERIMENTAL PROCEDURES

Parasites and Host Cells

Human foreskin fibroblast primary cells, and 293-TRex and J774 cell lines were cultured in DMEM (Invitrogen) supplemented with 10% heat-inactivated fetal bovine serum (Invitrogen), 10 mM HEPES buffer (pH 7.2), 2 mM L-glutamine, and 50 μg/mL penicillin and streptomycin (Invitrogen). Cells were incubated at 37°C in 5% CO_2. The *Toxoplasma* strains used in this study were RHku80 WT and RHku80 Δgra24 (Braun et al., 2013).

Reagents

Antibodies against HA (3F10; Roche), p38 MAPK (Cell Signaling Technology), Phospho-p38 MAPK (Cell Signaling Technology), Phospho-c-Fos (Ser32; Cell

Signaling Technology), H4 Acetylated (EMD Millipore), EGR1 (Cell Signaling Technology), Phospho-ATF-2 (Thr71; Cell Signaling Technology), and HAUSP (Bethyl Laboratories) were used in the immunofluorescence assay and/or in western blotting. Immunofluorescence secondary antibodies were coupled with Alexa Fluor 488 or Alexa Fluor 594 (Invitrogen). Secondary antibodies used in western blotting were conjugated to alkaline phosphatase (Promega). The p38 inhibitors were purchased from InvivoGen and Euromedex.

Cloning, Expression, and Purification

DNA encoding human p38α was synthesized (ShineGene Bio-Technologies) and cloned into pETBS with an N-terminal His_6-tag with a thrombin cleavage site. The mutant p38αK53R was obtained by PCR-based mutagenesis and verified by sequencing. Recombinant p38α and p38αK53R were expressed and purified following the same protocol. Both proteins were expressed in *E. coli* BL21 Rosetta2 cells (Novagen/Merck). Cells were lysed in lysis buffer (50 mM Tris [pH 7.4], 500 mM NaCl, 10 mM $MgCl_2$, 1 mM DTT, 5% glycerol, and 10 mM imidazole) by mild sonication and the lysate was loaded onto a pre-packed His trap column (GE Healthcare). Protein was eluted with a linear gradient to 500 mM imidazole. Cleavage of the His_6-tag was performed with thrombin overnight at 4°C in lysis buffer. After separation of cleaved and uncleaved protein, samples were further purified by size-exclusion chromatography using a HiLoad 16/60 Superdex 200 pg column (GE Healthcare) in buffer A (50 mM Tris [pH 7.4], 50 mM NaCl, 10 mM $MgCl_2$, 1 mM DTT, and 5% glycerol). Finally, the protein was loaded onto a Mono Q 5/50 GL (GE Healthcare) with a gradient to 1 M NaCl. This final step was necessary in order to separate the mono-phosphorylated protein from unphosphorylated protein. The protein was then concentrated to 10 mg/mL and stored at −20°C.

DNA encoding *T. gondii* GRA24 N-terminal truncation (GRA24ΔN) was synthesized (ShineGene Bio-Technologies) and cloned into pET28a using an N-terminal His_6-tag with a thrombin cleavage site. BL21-CondonPlus(DE3)-RIL cells transformed with pETBS p38α were then additionally transformed with pET28a GRA24ΔN. Co-expression of p38α and GRA24ΔN was induced overnight at 18° with 0.2 mM isopropyl-thio-β-D-galactoside. Cells were lysed in lysis buffer (50 mM Tris [pH 8.0] and 250 mM NaCl) by mild sonication, and the lysate was loaded onto a pre-packed His trap column (GE Healthcare) in buffer A (50 mM Tris [pH 8.0], 250 mM NaCl, and 20 mM imidazole). The complex was eluted with a linear gradient to 300 mM imidazole. Pure fractions were pooled and dialyzed against buffer B (50 mM Tris [pH 7.0] and 50 mM NaCl) overnight and subsequently loaded onto a 5 mL HiTrap Q column (GE Healthcare) and eluted with a gradient to 1 M NaCl where the complex eluted as a single peak. The complex was then further purified by size-exclusion chromatography using a HiLoad 16/60 Superdex 200 pg column (GE Healthcare) in buffer C (50 mM Tris [pH 7.4], 50 mM NaCl, and 5% glycerol).

The mutations in GRA24 were introduced in plasmids pcDNA-GRA24 WT-HA-Flag (HF) with the QuikChange Lightning Site-Directed Mutagenesis Kit (Stratagene). The following oligonucleotides for deletion of KIM sequence in the backbone vector pcDNA-GRA24 WT-HF vector (Braun et al., 2013) were used: GRA24del506-515 (5′-AGA CTG GTC TTC TTG AGC GCA TCG TTA AAC CAC C-3′), GRA24del506-515-antisense 5′-GGT GGT TTA ACG ATG CGC TCA AGA AGA CCA GTC T-3′), GRA24del427-436 (5′-GAC TGG TCT TCT TGA GTA CAT CCC TCG TCC TC-3′), and GRA24del427-436-antisense (5′-GAG GAC GAG GGA TGT ACT CAA GAA GAC CAG TC-3′). The resulting plasmids were pcDNA-GRA24ΔKIM1, pcDNA-GRA24ΔKIM2, and pcDNA-GRA24ΔKIM1/ΔKIM2, respectively.

Isothermal Titration Calorimetry

ITC was performed at 25°C using an iTC200 System (MicroCal, GE Healthcare). WT p38α or mutant proteins were dialyzed against the titration buffer (50 mM Tris [pH 7.0], 50 mM NaCl, and 1 mM DTT). MKK6 and GRA24 KIM peptides were also prepared in the same buffer. A 70 μM protein solution was titrated using 26 stepwise injections of 1.5 μL with each of the peptide solutions placed in the syringe. The GRA24 KIM peptide was used at 0.5 mM and the MKK6 peptide at 10 mM, the latter due to significantly lower affinity. The heat generated after each ligand injection was measured on the integral of the calorimetric signal. The resulting binding isotherms were analyzed by a nonlinear least-squares fit of the experimental data to a single site model (Turnbull and Daranas, 2003; Wiseman et al., 1989) using Microcal Origin 7.0 software. Experiments were duplicated and variability estimated to be 5% in the binding enthalpy and 10% for both the binding affinity and the number of sites.

In Vitro Kinase Assay

Auto-phosporylation of the GRA24KIM-p38α complex was analyzed using a radioactivity-based assay. The complex (1.2 μg) was pretreated with λ-phosphatase (New England Biolabs) and incubated with 5 mM $MgCl_2$ and 10 mM ATP (10:1 ATP-γP^{32}) at room temperature. Reactions were run for 30 min and stopped by adding SDS-PAGE loading buffer. Samples were run on 12% SDS-PAGE and then exposed to film to visualize the extent of incorporation of P^{32}.

ATF2 Assay

Kinase reactions were performed in the presence of 100 μM ATP and 1 μg of ATF-2 fusion protein as a substrate. The phosphorylation of ATF-2 at Thr71 was measured by western blot using a Phospho-ATF-2 (Thr71) Antibody.

In Vivo Inhibition Assays

Specific pharmacological inhibition of GRA24-dependent p38α phosphorylation in J774 MØ was monitored following 18 hr of infection with RHku80 and RHku80 Δgra24 strains and by using specific p38 inhibitors, control inhibitors, and DMSO vehicle.

293-TRex Transfection

Twenty-four hours before transfection, cells were plated (80% confluency) in six-well tissue culture dishes. Flag-fusion protein-expressing plasmids (1 μg) and 0.1 μg puromycin selection plasmid were co-transfected into 293-TRex cells with Lipofectamine reagent (Invitrogen) according to the manufacturer's instructions. Seventy-two hours later, cells were diluted in the presence of 5 μg/mL puromycin (Sigma-Aldrich) for selection. Individual drug-resistant clones were expanded and tested for tetracycline-inducible gene expression.

Crystallization

Crystallization conditions were established at the EMBL High Throughput Crystallization Laboratory (Grenoble, France). To obtain crystals of p38α in complex with the KIM peptide from GRA24 (GRA24KIM1-p38α) protein was incubated overnight at 4°C with a 3-fold molar excess of peptide GLLERRGV SELPPLYI (Eurogentec). The complex was then mixed 1:1 with 0.2 M $MgCl_2$, 0.1 M Tris/HCl (pH 8.5), and 25%–28% PEG 3350 and set up in sitting-drop plates. Crystals were harvested directly from the mother liquor (Pellegrini et al., 2011) using a MicroMesh loop (MiTeGen), plunged into liquid nitrogen, and stored at 70 K.

For p38αK53R in complex with the MKK6 peptide (MKK6KIM-p38αK53R), protein was incubated overnight at 4°C with a 3-fold molar excess of peptide SKGKKRNPGLKIPKA (Eurogentec). Crystals were obtained as above but equilibrated against a buffer containing 25% (w/v) PEG 3350 and 0.1 mM Bis-Tris (pH 6.5). Crystals were transferred to a cryoprotection buffer, prepared as described above (reservoir supplemented with 20% [v/v] PEG 400) and harvested using a MicroMesh loop, plunged into liquid nitrogen, and stored at 70 K.

Data Collection and Structure Solution

Diffraction data were collected at beamline ID23-2 (Flot et al., 2010) at the ESRF (Grenoble, France) on a MAR225 charge-coupled device detector to between 2.4 and 2.8 Å resolution. Crystals of MKK6KIM-p38αK53R formed long needles (with approximate dimensions of 100 × 20 × 20 μm^3) that were difficult to visualize. Crystals of the GRA24KIM-p38α complex were 500 μm in the largest dimension and displayed considerable heterogeneity in diffraction quality (Bowler and Bowler, 2014). Crystals were centered using automated mesh scans (Bowler et al., 2010; Brockhauser et al., 2012; Gabadinho et al., 2010; Svensson et al., 2015). The MKK6KIM-p38αK53R complex crystallized in the trigonal space group $P3_12_1$, with one molecule in the asymmetric unit and the GRA24KIM-p38α complex crystallized in the triclinic space group $P1$ with two molecules in the asymmetric unit (Table 1). Data were processed with XDS (Kabsch, 2010) and programs from the Collaborative Computational Project Number 4 suite (Winn et al., 2011). The structures were solved by molecular replacement using MolRep (Vagin and Teplyakov, 2010). For the p38αK53R structure (PDB: 1WFC; Jin et al., 2012) was used as a search model

with all water molecules removed. For the p38α and MKK6KIM-p38αK53R structures, the p38αK53R structure was used as a search model. Refinement was carried out alternately using Phenix (Afonine et al., 2012) and by manual rebuilding with COOT (Emsley and Cowtan, 2004). For the GRA24KIM-p38α complex, tight NCS restraints between monomers in the asymmetric unit were used at the beginning of refinement. Models were validated using MolProbity (Chen et al., 2010).

SAXS Experiments

SAXS data were collected at the bioSAXS beamline BM29 (Pernot et al., 2013) at the ESRF with a PILATUS 1 M detector (Dectris) at a wavelength of 0.992 Å and a camera length of 2.87 m. Scattering curves were measured from solutions of p38α without substrates, in complex with the GRA24 peptide, and of the GRA24KIM-p38α complex. Measurements were performed at protein concentrations between 2 and 15 mg/mL to verify that any inter-particle effects that may have been present could be accounted for and rule out their influence on the analysis. To exclude the possibility of radiation damage, ten frames, each of 1 s duration, were collected while continuously exposing fresh samples to the beam, the resulting frames were then compared to ensure that no differences in the SAXS profiles were induced by exposure to X-rays. All data were processed using the ATSAS program package (Petoukhov and Svergun, 2007). Radii of gyration (R_g) were evaluated from Guinier plots using PRIMUS (Konarev et al., 2003) and pair distance distribution functions, *P(r)*, were computed with GNOM (Svergun, 1992). The model of the GRA24KIM-p38α complex was refined using CORAL (Petoukhov et al., 2012).

Electron Microscopy

The GRA24KIM-p38α complex was absorbed to the clean side of a carbon film on mica, stained with 2% sodium silicotungstate, and transferred to a 400-mesh copper grid. The images were taken under low-dose conditions (<10 $e^-/Å^2$) at a nominal magnification of 49,000× with defocus values between 1.2 and 2.5 μm on an FEI Tecnai 12 electron microscope at 120 kV accelerating voltage using Kodak S0-163 films. Four micrographs were scanned with a Zeiss scanner at 7 μm pixel size (3.2 Å on the sample scale). Using EMAN2 (Tang et al., 2007), 237 views of the complex were selected, interactively boxed into 200 × 200 pixel boxes. Class averages were produced using IMAGIC (van Heel et al., 1996).

Atomic Force Microscopy

Samples were adsorbed to mica plates at a concentration of 0.1 mg/mL. A Chypher AFM (Asylum Research, Oxford Instruments) was used with MSNL cantilevers (Bruker) in AFM amplitude modulation mode.

ACCESSION NUMBERS

Coordinates and structure factors have been deposited in the PDB under accession codes PDB: 5ETA and 5ETF for the GRA24KIM1-p38α and MKK6KIM-p38αK53R structures, respectively. Correspondence and requests for materials should be addressed to H.B. (belrhali@embl.fr), M.A.H. (mohamed-ali.hakimi@ujf-grenoble.fr), or M.W.B. (mbowler@embl.fr).

SUPPLEMENTAL INFORMATION

Supplemental Information includes five figures, three tables, and two movies and can be found with this article online at http://dx.doi.org/10.1016/j.str.2016.10.011.

AUTHOR CONTRIBUTIONS

H.B., M.W.B., and M.A.H. designed the study. E.P. and U.K. expressed, purified, and crystallized proteins. E.P., H.B., and M.W.B. collected diffraction data and refined the structures. M.W.B collected and analyzed SAXS, EM, and AFM data. A.P. and E.P. performed ITC experiments and L.B., A.B., and M.A.H. performed experiments in *T. gondii*. E.P., A.P., H.B., M.A.H., and M.W.B analyzed the data. E.P., M.A.H., and M.W.B. wrote the paper. All authors discussed the results and implications and commented on the manuscript at all stages.

ACKNOWLEDGMENTS

This work was supported by the European Molecular Biology Laboratory (to E.P., A.P., H.B., and M.W.B.), M.A.H. and L.B. are supported by the European Research Council (ERC Consolidator grant no. 614880 Hosting TOXO) and the LabEx ParaFrap (ANR-11-LABX-0024). A.B. was supported by the ANR Jeune Chercheur 2012 ToxoEffect (ANR- 12-JSV3–0004-01). This work used the platforms of the Grenoble Instruct Centre (ISBG; UMS 3518 CNRS-CEA-UJF-EMBL) with support from FRISBI (ANR-10-INSB-05-02) and GRAL (ANR-10-LABX-49-01) within the Grenoble Partnership for Structural Biology (PSB). We thank Adam Round and Taiana Maia de Olivera (EMBL Grenoble) for helpful discussions on SAXS and EM, respectively. Luca Costa (ESRF) is thanked for assistance with AFM. We are also indebted to the EMBL Heidelberg Core Facilities, particularly Joanna Kirkpatrick (MS analysis) and Hüseyin Besir (Protein Expression and Purification).

Received: May 19, 2016
Revised: September 21, 2016
Accepted: October 25, 2016
Published: November 23, 2016

REFERENCES

Afonine, P.V., Grosse-Kunstleve, R.W., Echols, N., Headd, J.J., Moriarty, N.W., Mustyakimov, M., Terwilliger, T.C., Urzhumtsev, A., Zwart, P.H., and Adams, P.D. (2012). Towards automated crystallographic structure refinement with phenix.refine. Acta Crystallogr. D Biol. Crystallogr. *68*, 352–367.

Akella, R., Min, X., Wu, Q., Gardner, K.H., and Goldsmith, E.J. (2010). The third conformation of p38alpha MAP kinase observed in phosphorylated p38alpha and in solution. Structure *18*, 1571–1578.

Bellon, S., Fitzgibbon, M.J., Fox, T., Hsiao, H.M., and Wilson, K.P. (1999). The structure of phosphorylated p38gamma is monomeric and reveals a conserved activation-loop conformation. Structure *7*, 1057–1065.

Bowler, M.G., and Bowler, M.W. (2014). Measurement of the intrinsic variability within protein crystals: implications for sample-evaluation and data-collection strategies. Acta Crystallogr. F Struct. Biol. Commun. *70*, 127–132.

Bowler, M.W., Guijarro, M., Petitdemange, S., Baker, I., Svensson, O., Burghammer, M., Mueller-Dieckmann, C., Gordon, E.J., Flot, D., McSweeney, S.M., and Leonard, G.A. (2010). Diffraction cartography: applying microbeams to macromolecular crystallography sample evaluation and data collection. Acta Crystallogr. D Biol. Crystallogr. *66*, 855–864.

Braun, L., Brenier-Pinchart, M.-P., Yogavel, M., Curt-Varesano, A., Curt-Bertini, R.-L., Hussain, T., Kieffer-Jaquinod, S., Coute, Y., Pelloux, H., Tardieux, I., et al. (2013). A Toxoplasma dense granule protein, GRA24, modulates the early immune response to infection by promoting a direct and sustained host p38 MAPK activation. J. Exp. Med. *210*, 2071–2086.

Brockhauser, S., Svensson, O., Bowler, M.W., Nanao, M., Gordon, E., Leal, R.M., Popov, A., Gerring, M., McCarthy, A.A., and Gotz, A. (2012). The use of workflows in the design and implementation of complex experiments in macromolecular crystallography. Acta Crystallogr. D Biol. Crystallogr. *68*, 975–984.

Brown, M.D., and Sacks, D.B. (2009). Protein scaffolds in MAP kinase signalling. Cell Signal. *21*, 462–469.

Chang, C.I., Xu, B.E., Akella, R., Cobb, M.H., and Goldsmith, E.J. (2002). Crystal structures of MAP kinase p38 complexed to the docking sites on its nuclear substrate MEF2A and activator MKK3b. Mol. Cell *9*, 1241–1249.

Chen, Z., Gibson, T.B., Robinson, F., Silvestro, L., Pearson, G., Xu, B., Wright, A., Vanderbilt, C., and Cobb, M.H. (2001). MAP kinases. Chem. Rev. *101*, 2449–2476.

Chen, V.B., Arendall, W.B., 3rd, Headd, J.J., Keedy, D.A., Immormino, R.M., Kapral, G.J., Murray, L.W., Richardson, J.S., and Richardson, D.C. (2010). MolProbity: all-atom structure validation for macromolecular crystallography. Acta Crystallogr. D Biol. Crystallogr. *66*, 12–21.

Cobb, M.H., and Goldsmith, E.J. (1995). How MAP kinases are regulated. J. Biol. Chem. *270*, 14843–14846.

Davey, N.E., Van Roey, K., Weatheritt, R.J., Toedt, G., Uyar, B., Altenberg, B., Budd, A., Diella, F., Dinkel, H., and Gibson, T.J. (2012). Attributes of short linear motifs. Mol. Biosys. *8*, 268–281.

Davis, R.J. (1995). Transcriptional regulation by MAP kinases. Mol. Rep. Dev. *42*, 459–467.

De Nicola, G.F., Martin, E.D., Chaikuad, A., Bassi, R., Clark, J., Martino, L., Verma, S., Sicard, P., Tata, R., Atkinson, R.A., et al. (2013). Mechanism and consequence of the autoactivation of p38alpha mitogen-activated protein kinase promoted by TAB1. Nat. Struct. Mol. Biol. *20*, 1182–1190.

Desagher, S., Osen-Sand, A., Montessuit, S., Magnenat, E., Vilbois, F., Hochmann, A., Journot, L., Antonsson, B., and Martinou, J.-C. (2001). Phosphorylation of bid by casein kinases I and II regulates its cleavage by caspase 8. Mol. Cell *8*, 601–611.

Diskin, R., Lebendiker, M., Engelberg, D., and Livnah, O. (2007). Structures of p38α active mutants reveal conformational changes in L16 loop that induce autophosphorylation and activation. J. Mol. Biol. *365*, 66–76.

Døskeland, A.P., Martinez, A., Knappskog, P.M., and Flatmark, T. (1996). Phosphorylation of recombinant human phenylalanine hydroxylase: effect on catalytic activity, substrate activation and protection against non-specific cleavage of the fusion protein by restriction protease. Biochem. J. *313*, 409–414.

Elde, N.C., and Malik, H.S. (2009). The evolutionary conundrum of pathogen mimicry. Nat. Rev. Microbiol. *7*, 787–797.

Emsley, P., and Cowtan, K. (2004). Coot: model-building tools for molecular graphics. Acta Crystallogr. D Biol. Crystallogr. *60*, 2126–2132.

Enslen, H., Brancho, D.M., and Davis, R.J. (2000). Molecular determinants that mediate selective activation of p38 MAP kinase isoforms. EMBO J. *19*, 1301–1311.

Flot, D., Mairs, T., Giraud, T., Guijarro, M., Lesourd, M., Rey, V., van Brussel, D., Morawe, C., Borel, C., Hignette, O., et al. (2010). The ID23-2 structural biology microfocus beamline at the ESRF. J. Synchrotron. Radiat. *17*, 107–118.

Francis, D.M., Rozycki, B., Koveal, D., Hummer, G., Page, R., and Peti, W. (2011). Structural basis of p38alpha regulation by hematopoietic tyrosine phosphatase. Nat. Chem. Biol. *7*, 916–924.

Fuxreiter, M., Tompa, P., and Simon, I. (2007). Local structural disorder imparts plasticity on linear motifs. Bioinformatics *23*, 950–956.

Gabadinho, J., Beteva, A., Guijarro, M., Rey-Bakaikoa, V., Spruce, D., Bowler, M.W., Brockhauser, S., Flot, D., Gordon, E.J., Hall, D.R., et al. (2010). MxCuBE: a synchrotron beamline control environment customised for macromolecular crystallography experiments. J. Synchrotron. Radiat. *17*, 700–707.

Garai, A., Zeke, A., Gogl, G., Toro, I., Fordos, F., Blankenburg, H., Barkai, T., Varga, J., Alexa, A., Emig, D., et al. (2012). Specificity of linear motifs that bind to a common mitogen-activated protein kinase docking groove. Sci. Signal. *5*, ra74.

Gavin, A.C., and Nebreda, A.R. (1999). A MAP kinase docking site is required for phosphorylation and activation of p90(rsk)/MAPKAP kinase-1. Curr. Biol. *9*, 281–284.

Gum, R.J., and Young, P.R. (1999). Identification of two distinct regions of p38 MAPK required for substrate binding and phosphorylation. Biochem. Biophys. Res. Commun. *266*, 284–289.

Hagai, T., Azia, A., Babu, M.M., and Andino, R. (2014). Use of host-like peptide motifs in viral proteins is a prevalent strategy in host-virus interactions. Cell Rep. *7*, 1729–1739.

Hakimi, M.A., and Bougdour, A. (2015). Toxoplasma's ways of manipulating the host transcriptome via secreted effectors. Curr. Opin. Microbiol. *26*, 24–31.

Heo, Y.S., Kim, S.K., Seo, C.I., Kim, Y.K., Sung, B.J., Lee, H.S., Lee, J.I., Park, S.Y., Kim, J.H., Hwang, K.Y., et al. (2004). Structural basis for the selective inhibition of JNK1 by the scaffolding protein JIP1 and SP600125. EMBO J. *23*, 2185–2195.

Hunter, C.A., and Sibley, L.D. (2012). Modulation of innate immunity by *Toxoplasma gondii* virulence effectors. Nat. Rev. Microbiol. *10*, 766–778.

Jin, Y., Cliff, M.J., Baxter, N.J., Dannatt, H.R., Hounslow, A.M., Bowler, M.W., Blackburn, G.M., and Waltho, J.P. (2012). Charge-balanced metal fluoride complexes for protein kinase A with adenosine diphosphate and substrate peptide SP20. Angew. Chem. *51*, 12242–12245.

Johnson, G.L., and Lapadat, R. (2002). Mitogen-activated protein kinase pathways mediated by ERK, JNK, and p38 protein kinases. Science *298*, 1911–1912.

Jura, N., Zhang, X., Endres, N.F., Seeliger, M.A., Schindler, T., and Kuriyan, J. (2011). Catalytic control in the EGF receptor and its connection to general kinase regulatory mechanisms. Mol. Cell *42*, 9–22.

Kabsch, W. (2010). XDS. Acta Crystallogr. D Biol. Crystallogr. *66*, 125–132.

Kallunki, T., Deng, T.L., Hibi, M., and Karin, M. (1996). c-jun Can recruit JNK to phosphorylate dimerization partners via specific docking interactions. Cell *87*, 929–939.

Khokhlatchev, A.V., Canagarajah, B., Wilsbacher, J., Robinson, M., Atkinson, M., Goldsmith, E., and Cobb, M.H. (1998). Phosphorylation of the MAP kinase ERK2 promotes its homodimerization and nuclear translocation. Cell *93*, 605–615.

Kim, L., Del Rio, L., Butcher, B.A., Mogensen, T.H., Paludan, S.R., Flavell, R.A., and Denkers, E.Y. (2005). p38 MAPK autophosphorylation drives macrophage IL-12 production during intracellular infection. J. Immunol. *174*, 4178–4184.

Konarev, P.V., Volkov, V.V., Sokolova, A.V., Koch, M.H.J., and Svergun, D.I. (2003). PRIMUS: a Windows PC-based system for small-angle scattering data analysis. J. Appl. Crystallogr. *36*, 1277–1282.

Kornev, A.P., and Taylor, S.S. (2010). Defining the conserved internal architecture of a protein kinase. Biochem. Biophys. Acta *1804*, 440–444.

Lee, S.J., Zhou, T., and Goldsmith, E.J. (2006). Crystallization of MAP kinases. Methods *40*, 224–233.

McClendon, C.L., Kornev, A.P., Gilson, M.K., and Taylor, S.S. (2014). Dynamic architecture of a protein kinase. Proc. Natl. Acad. Sci. USA *111*, E4623–E4631.

Melo, M.B., Jensen, K.D., and Saeij, J.P. (2011). *Toxoplasma gondii* effectors are master regulators of the inflammatory response. Trends Parasitol. *27*, 487–495.

Nardozzi, J.D., Lott, K., and Cingolani, G. (2010). Phosphorylation meets nuclear import: a review. Cell Commun. Signal. *8*, 1–17.

Pellegrini, E., Piano, D., and Bowler, M.W. (2011). Direct cryocooling of naked crystals: are cryoprotection agents always necessary? Acta Crystallogr. D Biol. Crystallogr. *67*, 902–906.

Pernot, P., Round, A., Barrett, R., De Maria Antolinos, A., Gobbo, A., Gordon, E., Huet, J., Kieffer, J., Lentini, M., Mattenet, M., et al. (2013). Upgraded ESRF BM29 beamline for SAXS on macromolecules in solution. J. Synchrotron. Radiat. *20*, 660–664.

Peti, W., and Page, R. (2013). Molecular basis of MAP kinase regulation. Protein Sci. *22*, 1698–1710.

Petoukhov, M.V., and Svergun, D.I. (2007). Analysis of X-ray and neutron scattering from biomacromolecular solutions. Curr. Opin. Struct. Biol. *17*, 562–571.

Petoukhov, M.V., Franke, D., Shkumatov, A.V., Tria, G., Kikhney, A.G., Gajda, M., Gorba, C., Mertens, H.D.T., Konarev, P.V., and Svergun, D.I. (2012). New developments in the ATSAS program package for small-angle scattering data analysis. J. Appl. Crystallogr. *45*, 342–350.

Sharrocks, A.D., Yang, S.H., and Galanis, A. (2000). Docking domains and substrate-specificity determination for MAP kinases. Trends Biochem. Sci. *25*, 448–453.

Smith, J.A., Poteet-Smith, C.E., Malarkey, K., and Sturgill, T.W. (1999). Identification of an extracellular signal-regulated kinase (ERK) docking site in ribosomal S6 kinase, a sequence critical for activation by ERK in vivo. J. Biol. Chem. *274*, 2893–2898.

Svensson, O., Malbet-Monaco, S., Popov, A., Nurizzo, D., and Bowler, M.W. (2015). Fully automatic characterization and data collection from crystals of biological macromolecules. Acta Crystallogr. D Biol. Crystallogr. *71*, 1757–1767.

Svergun, D.I. (1992). Determination of the regularization parameter in indirect-transform methods using perceptual criteria. J. Appl. Crystallogr. *25*, 495–503.

Szafranska, A.E., Luo, X., and Dalby, K.N. (2005). Following in vitro activation of mitogen-activated protein kinases by mass spectrometry and tryptic

peptide analysis: purifying fully activated p38 mitogen-activated protein kinase α. Anal. Biochem. *336*, 1–10.

Tang, G., Peng, L., Baldwin, P.R., Mann, D.S., Jiang, W., Rees, I., and Ludtke, S.J. (2007). EMAN2: an extensible image processing suite for electron microscopy. J. Struct. Biol. *157*, 38–46.

Tanoue, T., Maeda, R., Adachi, M., and Nishida, E. (2001). Identification of a docking groove on ERK and p38 MAP kinases that regulates the specificity of docking interactions. EMBO J. *20*, 466–479.

Tokunaga, Y., Takeuchi, K., Takahashi, H., and Shimada, I. (2014). Allosteric enhancement of MAP kinase p38alpha's activity and substrate selectivity by docking interactions. Nat. Struct. Mol. Biol. *21*, 704–711.

Turnbull, W.B., and Daranas, A.H. (2003). On the value of c: can low affinity systems be studied by isothermal titration calorimetry? J. Am. Chem. Soc. *125*, 14859–14866.

Vagin, A., and Teplyakov, A. (2010). Molecular replacement with MOLREP. Acta Crystallogr. D Biol. Crystallogr. *66*, 22–25.

van Heel, M., Harauz, G., Orlova, E.V., Schmidt, R., and Schatz, M. (1996). A new generation of the IMAGIC image processing system. J. Struct. Biol. *116*, 17–24.

Winn, M.D., Ballard, C.C., Cowtan, K.D., Dodson, E.J., Emsley, P., Evans, P.R., Keegan, R.M., Krissinel, E.B., Leslie, A.G., McCoy, A., et al. (2011). Overview of the CCP4 suite and current developments. Acta Crystallogr. D Biol. Crystallogr. *67*, 235–242.

Wiseman, T., Williston, S., Brandts, J.F., and Lin, L.N. (1989). Rapid measurement of binding constants and heats of binding using a new titration calorimeter. Anal. Biochem. *179*, 131–137.

Zakowski, V., Keramas, G., Kilian, K., Rapp, U.R., and Ludwig, S. (2004). Mitogen-activated 3p kinase is active in the nucleus. Exp. Cell Res. *299*, 101–109.

Zeke, A., Bastys, T., Alexa, A., Garai, Á., Mészáros, B., Kirsch, K., Dosztányi, Z., Kalinina, O.V., and Reményi, A. (2015). Systematic discovery of linear binding motifs targeting an ancient protein interaction surface on MAP kinases. Mol. Sys. Biol. *11*, 837.

Zhou, T., Sun, L., Humphreys, J., and Goldsmith, E.J. (2006). Docking interactions induce exposure of activation loop in the MAP kinase ERK2. Structure *14*, 1011–1019.

Zuniga, A., Torres, J., Ubeda, J., and Pulido, R. (1999). Interaction of mitogen-activated protein kinases with the kinase interaction motif of the tyrosine phosphatase PTP-SL provides substrate specificity and retains ERK2 in the cytoplasm. J. Biol. Chem. *274*, 21900–21907.